Imaging simulations of selected science with the Magdalena Ridge Observatory Interferometer

Michelle Creech-Eakman[a], John Young[b], Chris Haniff[b], David Buscher[b], Martin Elvis[c], Andrea Chiavassa[d], Marc Schartmann[e]
[a]New Mexico Tech, Department of Physics, Socorro, NM, USA, 87801;
[b]Cavendish Laboratory, J.J.Thomson Avenue, Cambridge, UK, CB3 0HE;
[c]Harvard-Smithsonian Center for Astrophysics, 60 Garden Street, Cambridge, Massachusetts, USA 02138
[d]Max Planck Institute for Astrophysics, Karl-Schwarzschild-Strass-1, Garching, Germany, 85741;
[e]Max Planck Institute for Extraterrestrial Physics, Giessenbachstrasse, Garching, Germany, 85748

ABSTRACT

We present simulated observations of surface features on Red Supergiant (RSG) stars and clumpy dust structures surrounding Active Galactic Nuclei (AGN) with the Magdalena Ridge Observatory Interferometer (MROI). These represent two of the classes of astrophysical targets enumerated in the MROI Key Science Mission that are typical of the types of complex astrophysical phenomena that the MROI has been designed to image. The simulations are based on source structures derived from recent theoretical models and include both random and systematic noise on the measured Fourier data (visibility amplitudes and closure phases) consistent with our expectations for typical such targets observed with the MROI. Image reconstructions, obtained using the BSMEM imaging package, are presented for 4-, 6- and 8-telescope implementations of the array. Although a rudimentary imaging capability is demonstrated with only 4 telescopes, the detailed features of targets are only reliably determined when at least 6 telescopes are present. By the tine 8 telescope are used, the reconstructed images are sufficiently faithful to allow the discrimination between competing models, confirming the design goal of the MROI, i.e. to offer model-independent near-infrared imaging on sub-milli-arcsecond scales.

Keywords: Long-baseline interferometry, infrared imaging, high angular resolution, image reconstruction, AGN, supergiant stars

1. INTRODUCTION

The Magdalena Ridge Observatory Interferometer [1] is a 10-element 1.4m interferometric imaging array working at optical and near-infrared wavelengths and scheduled for first fringes in 2012. The entire design of the interferometer is centered around one goal, to produce model-independent images of faint and complex astrophysical targets with sub-milliarcsecond spatial resolutions. Imaging with separated-element optical interferometers was first accomplished using the COAST array [2] but is only now becoming routinely available with arrays like CHARA and NPOI [3], [4]. At present images are still time-consuming to construct because only a few baselines can be reliably combined at once, and because the sensitivities and efficiencies of existing arrays are not high. As a result there are only a limited number of available targets. A recent map produced using MIRC [5] at CHARA of the enigmatic eclipsing system, Epsilon Aurigae [6], has demonstrated the remarkable potential for optical interferometry to contribute substantially to our understanding of astrophysical phenomena in a way that would not have been possible with lower spatial resolution techniques.

The ability for imaging to solve long-standing questions in astrophysics underscores the need for an imaging machine like the MROI. In this paper we demonstrate the MROI's imaging capabilities using models developed to explain other recent interferometric observations. Because the MROI Key Science Mission [7] will concentrate on faint and complex systems, and on making measurements of multiple targets of the same class, we have chosen two examples that are

major foci of our Key Science Mission – Active Galactic Nuclei (AGN) and red supergiants (RSG). Not only have the simulations relied upon realistic astrophysical models, but we have also used realistic noise, system performance, and apparent angular sizes to examine how the imaging capabilities of the MROI will vary as a function of the number of telescopes used.

In the next section we discuss the models themselves, while in section 3 we present our results. Our conclusions about the simulated MROI performance are given in Section 4

2. MODELING AND SIMULATION STRATEGY

Two model types were selected for exploration in this paper. Both were selected because they had already been used to help interpret recent interferometric observations, and so had been developed with the aim of modeling physics structures and phenomena that might be resolvable with very-high angular resolution techniques. In this paper we have restricted attention to the imaging performance of the MROI is its lowest spectral resolution mode (R~30) because it is in the mode that it will deliver its maximum sensitivity. In the simulations either 4, 6 or 8 telescopes in the MROI were assumed to have been used. In all cases spatial modulation of the fringes was assumed. For the 4- and 6-telescope simulations we assumed a 4-way beam combiner (switchable so that all 6 beams could be interfered in turn for the 6-telescope array), using a detector with 5e- readout noise RMS and with the H or K bands being spread over 128 separate pixels per spectral channel. For the 8-telescope simulations we assumed a similar switchable science beam combiner, but one which mixed 6 beams together simultaneously (using 192 pixels per spectral channel), and with a slightly better detector with 4e- readout noise. This is consistent with the current deployment plan for the MROI, which envisions an initial deployment of up to six telescopes in the near term, and subsequent enhancements in the future to expand the array to a 10-element configuration with second-generation instruments and an additional visible (RI-band) beam combiner.

Simulated datasets were prepared by evaluating the discrete Fourier transform of suitably scaled model images at spatial frequencies corresponding to the assumed MROI interferometric projected baselines. The targets were assumed to have the same structure across either the H or K spectral channels. The Fourier data were then used to generate the source visibilities and thereafter used to prepare "perfect" values of the relevant interferometric observables, i.e. squared visibilities and bispectra. These were subsequently adjusted – that is had errors incorporated – so as to properly mimic the signal to noise that would have been expected given various target magnitudes, the predicted interferometric performance, e.g. coherence losses due to jitter etc., and the assumed detector performance. In addition, calibration errors on the visibilities and closure phases were added. These were presumed uncorrelated and were at the level of $\Delta V^2/V^2 = 0.02$ and 0.8 degrees for the closure phases, which correspond to the modest design goals for the MROI.

Fig 1: An artist's impression of the Magdalena Ridge Observatory Interferometer when fully deployed. In this figure the 10 telescopes are in their highest resolution configuration which gives a maximum baseline of ~340m. The long delay-line building to the left points roughly east.

The MROI array is located at a latitude of +33.98 degrees, and its Y shaped layout offers baselines ranging from 7.5 to 340m (see Figure 1). The particular baselines chosen for each of the simulations were picked to mimic a 6-hour observation, with 100 seconds of incoherent observation time per measurement of source and calibrator, and the use of a single calibrator. No array reconfiguration was assumed. For the 4- and 6-telescope RSG cases, an optimum choice of telescope configuration was used so as to maximize the number of different uv-plane points and closure phase combinations collected. Otherwise, array layouts that allowed baseline bootstrapping (i.e. that had uniform spacings between neighboring telescopes) were selected. Importantly, the same nearest-neighborhood spacing was used regardless of the number of telescopes. As a result, the image reconstructions with 4-, 6- and 8-telescope bootstrapped data have slightly different angular resolutions.

All the model datasets were prepared in the IAU standard OIFITS formats [8], and were then used as input to the BSMEM maximum entropy imaging code [9]. We used a Gaussian default image for the AGN reconstructions, and a uniform disk default image for the red supergiants.

2.1 AGN models

For our AGN performance simulations, we used the model of Schartmann et al [10]. In this scenario, the purported "dust torus", which in the standard model for AGNs is assumed to shadow the nucleus proper, is assumed to be comprised of an assemblage of discrete clouds. i.e. it does not correspond to a smooth continuous distribution of dust. As a result some lines of sight to the more distant dust clouds may be obscured while others may not. The upshot of this is that the hottest dust, which in principle can be traced by its near IR continuum emission, can exist both very close to and distant from the nuclear core. This leads to a much clumpier near-IR brightness distribution than smooth dust torus models.

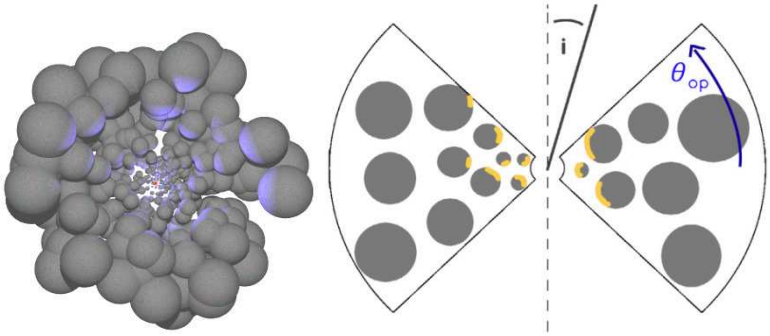

Fig 2: A schematic distribution of the dust clouds and AGN core assumed in the Schartmann et al. [10] model (left hand panel). The AGN core is the red dot at the center, while the pale blue regions show which clouds have direct lines of sight to the core and hence are heated. The left hand panel shows the geometry of one of the models used, and identified the opening angle of the cloud distribution as well as the locations of the hottest dust (yellow regions).

For this paper we assumed a "torus" opening angle of 45^{o} and let the dust clouds (which were assumed to follow the classic MRN-model [11]) be distributed randomly in radial position but follow a set of empirical relations in angle and distance from the black hole. All the cells in the discretized physical modeling code were assumed to contain a homogeneous distribution of dust with the same optical depth relation, but the cells were allowed to intersect one another to form clouds. Shear forces were also included in the model calculations and increased inwards, due to differential rotation within the AGN environment. To obtain the spectral energy distribution, temperature and surface brightness distributions of the resulting heated dust distribution the 3D radiative transfer code MC3D was employed [12]. For full details of the modeling the reader in encouraged to read Schartmann et al. [10] and references therein.

Surface brightness distributions were produced assuming both a pole-on and edge-on line of sight for the interferometer and the visibility and closure phase data were then generated assuming a central AGN core magnitude in the K band (2.2 microns) of 12.5. This gave integrated magnitudes for the dust fluxes of 10.6 and 10.8 respectively.

2.2 RSG models

For the RSG imaging simulations we used the model of Chiavassa et al [13]. This physical and radiative transfer code has been used to investigate how convection in red super-giant stars can create large-scale granulation which leads to significant surface inhomogeneities. The dynamical simulations of the stellar structure were created using CO^{5}BOLD [14] in the *star-in-a-box* configuration, using LTE radiative transfer and a grey Rosseland mean opacity, derived by interpolation of OPAL and PHOENIX data. Then, the OPTIM3D code, a 3D pure local thermodynamic equilibrium radiative transfer code with wavelength dependent treatment of opacities, was used to compute synthetic spectra and intensity maps from snapshots of the 3D hydrodynamical simulations. These maps include a realistic treatment of surface Doppler shifts caused by the convective motions and so can be used to produce maps of the stellar surface for both high and low spectral resolution simulations.

We chose a stellar model with the following physical parameters: mass: $12M_o$, luminosity: 9300 L_o, radius: 832 R_o and an effective temperature of 3490K. Full details of the model and modeling procedures can be found in Chiavassa et al. [13] and the references therein.

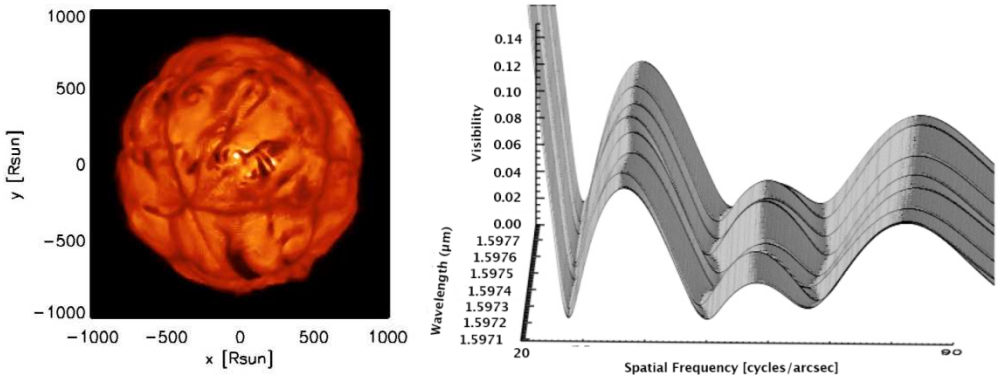

Fig 3: One of the instantaneous surface images produced by the stellar model (left hand panel) of Chiavassa et al. [13]. In this case the wavelength band has been chosen to isolate the near-IR CO bandhead which is a favorite target for interferometer arrays that have a near-infrared imaging capability such as the Keck Interferometer and VLTI arrays. The right hand panel shows the visibility amplitude as a function of wavelength and spatial frequency for the model.

3. IMAGE RECONSTRUCTION RESULTS

In the sub-sections below we present our image reconstructions for implementations of the MROI that utilize different numbers of unit telescopes ranging from 4 to 8. In each case we present the "truth" image, and then the 4-, 6- and 8-telescope inversions assuming the observation scenarios described above. In all cases, the truth image presented in each panel assumes the use of a perfect telescope with 3x the nominal resolution (λ/B_{max}) of the 8-element array. This is used as the baseline about which the different reconstructions are compared.

3.1 AGN results

As mentioned above, for the AGN simulations, we chose to model both a pole-on and an edge-on model. For the pole-on case, the AGN was assumed located at a distance of 60 Mpc, giving it an integrated K-band magnitude of 10.8. The edge on simulation assumed a distance of 30 Mpc and had a resulting integrated K-band magnitude of 10.6. The central AGN engine was assumed obscured for this edge-on case. The 6- and 8-telescope simulations assumed the use of a fast-

switchyard for the combinations, delivering 3 sets of interleaved observations taken as described above. The maximum baselines used in each case corresponded to spatial resolutions of 1.5, 1.9 and 3.7 milliarcseconds (mas) for the 8-, 6-, and 4-telescope configurations. The mean SNR per data point ranged from 4-6 for the AGN at 60 Mpc and from 6-10 for the AGN at 30 Mpc.

Figure 4 below shows in turn, the uv-plane coverage for the simulations, and below the reconstructions for the pole-on and edge-on AGN geometries. What is immediately apparent from the results is that the large scale geometric features of the truth image are recovered with moderate fidelity even with the 4-element array. This bodes very well for the capabilities for the initial deployment of the MROI. Not surprisingly, the imaging fidelity improves considerably as the number of telescopes increases and by the time an 8-element array is assumed, the imaging performance is largely limited by the uv-plane coverage rather than the signal-to-noise of the data, There are, of course, low level noise features in the 8-element reconstructions, but their repetitive structure in the map suggests their provenance.

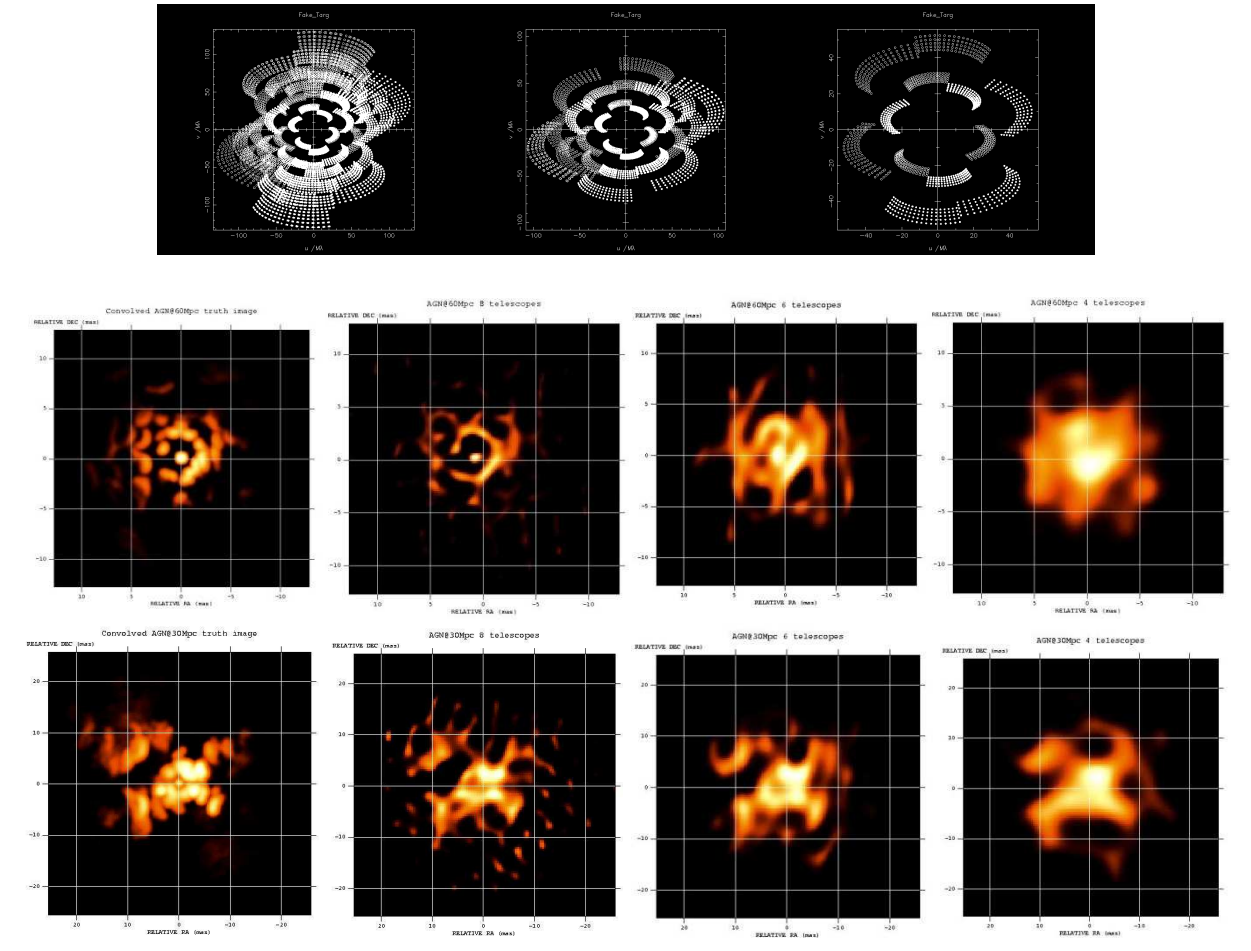

Fig 4: The uv-plane coverage (top panel) and image reconstruction results for the AGN simulations. The middle panel shows the results for the pole-on geometry (60 Mpc), while the lower panel corresponds to the edge-on torus (30 Mpc). In each row of the figure the number of telescopes assumed in the array goes from 8, to 6, to 4 from left to right, as is clearly seen in the relative degradation in the fidelity of the images. In the middle and lower panels the left-most image is a "truth" image recovered by convolving the original radiative transfer model with a Gaussian PSF corresponding to the use of a telescope with an angular resolution 3 times better than the 8-element array. Note that the color scale used in the images is logarithmic.

Perhaps the most exciting outcome of these results is the fact that the differentiation between the pole-on and edge-on geometries – which is most evident in the presence of a very bright unresolved core at the center of the image – is clearly apparent by the time 6 elements contribute to the array. With 8 telescopes even the detailed features of the disposition of the dust emission are faithfully recovered, and so these results suggest that major advances in our understanding of the response of a galactic core to an embedded black hole will be directly observable with the MROI.

3.2 RSG results

The red supergiant simulation mimics observations of a star similar to the archetype Betelgeuse (Alpha Orionis) but at 0.9 kpc. i.e. seven times further away than Betelgeuse, and hence with an apparent H magnitude of +0.2. We chose to simulate data for the H band because this is close to the stellar continuum and so effectively probes more deeply into the stellar atmosphere. The physical baselines used for the 8-, 6- and 4-telescope simulations corresponded to angular resolutions of 1.2, 1.7 and 1.7 mas respectively, while the mean signal to noise per data point ranged from 29 to 39.

Figure 5 below shows the truth image (see Section 3.1 for definition) to the left and the three different image reconstructions to the right. It is evident that even with only 4 telescopes the presence of surface inhomogeneities is detected. However, the surface structure is sufficiently complicated that it is only with an 8-telescope array that the recovered image shows the correct locations of the major hot- and cold-spots. It is likely that for this type of target a combination of imaging and subsequent model-fitting would be the best strategy to determine quantitatively the characteristics of the stellar surface.

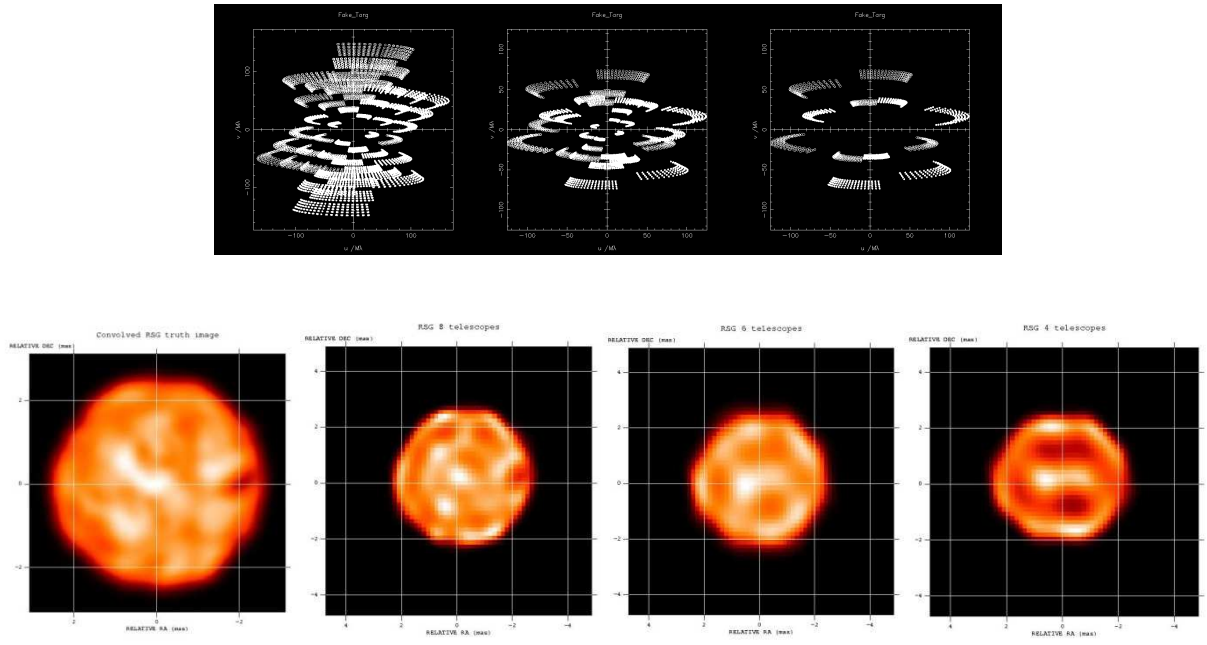

Fig 5: The top most panel shows the uv-plane coverage for the 8-, 6- and 4- telescope arrays used for the RSG simulations. In the second layer, truth image (left – at 3x resolution of the 8-element reconstruction) and image reconstructions (right three panels for 8-, 6- and 4- telescopes respectively) for the red supergiant simulations are shown. Unlike the somewhat simpler structure of the AGN, it is only when 8 telescopes are used that the imaging faithfully recovers most of the stellar surface structure. Still, inhomogeneities and a stellar bulge on the left of the image are evident even with only 4 telescopes. Note that the color scale used in the images is linear in this presentation.

4. CONCLUSIONS

We have presented results, obtained using realistic physical models and representative simulated noisy interferometric data that demonstrate the powerful imaging capability expected for the Magdalena Ridge Observatory Interferometer. Image reconstructions of the near-IR emitting structures of both AGN and supergiant star surfaces are clearly mapped with 4-, 6-, and 8-telescope deployments of the array. Although interferometry with 4 unit telescopes delivers only a rudimentary imaging capability, it is still enough to distinguish between different theoretical scenarios for relatively simple targets. For highly complex targets, such as the surface of a fully convective supergiant, more telescopes are needed, perhaps as many as 8. The number of AGN accessible to the MROI given its limiting sensitivity of H=14 is roughly 100, and of these perhaps 25% will be at distances of order 50 Mpc, i.e. corresponding to the distances assumed for these simulations. At this sensitivity and angular resolution level, the sample of available supergiant stars will likely be an order of magnitude greater, though it will be limited by the angular resolution available since RSGs are so luminous that any one that can be resolved will be bright enough to map). Imaging of such samples with the level of fidelity and angular resolution demonstrated here is likely to be a transformational step in contemporary astrophysics.

REFERENCES

[1] Creech-Eakman, M. et al., "Magdalena Ridge Observatory Interferometer: advancing to first light and new science", Proceedings SPIE, 7734, 5 (2010).

[2] Baldwin, J. E. and 15 coauthors, "The first images from an optical aperture synthesis array: mapping of Capella with COAST at two epochs", Astronomy and Astrophysics, 306, L13 (1996).

[3] ten Brummelaar, T. A., McAlister, H. A., et al., "An update on the CHARA Array", Proceedings SPIE, 7734, 2 (2010)

[4] Hutter, D. J. and 13 coauthors, "NPOI: recent progress and future prospects", Proceedings SPIE, 7013, 5 (2008).

[5] Monnier, J. D. and 12 coauthors, "Michigan Infrared Combiner (MIRC): Commissioning results at the CHARA array", Proceedings SPIE, 6268, 55 (2006).

[6] Kloppenborg, B. Stencel, R. E., and 15 coauthors, "Infrared images of the transiting disk in the Epsilon Aurigae System", Nature, 464, 870 (2010).

[7] Creech-Eakman, M. J., Buscher, D. F., Haniff, C. A., Romero, V. D., "The Magdalena Ridge Observatory Interferometer: a fully optimized aperture synthesis array for imaging", Proceedings SPIE, 5491, 405 (2004).

[8] Pauls, T., Young, J., Cotton, W., Monnier, J. D.," A data exchange standard for optical (visible/IR) interferometry" Publications of the Astronomical Society of the Pacific, 17, 1255 (2005).

[9] Baron, F. and Young, J. S., "Image reconstruction at Cambridge University", Proceedings SPIE, 7013, 121 (2008).

[10] Schartmann, M., Meisenheimer, K., Camenzind, M., Wolf, S., Tristam, K., Henning, T, "Three-dimensional radiative transfer models of clumpy tori in Seyfert galaxies" Astronomy and Astrophysics, 482, 67 (2008)

[11] Mathis, J, Rumpl, W., Nordsieck, K., "The size distribution of interstellar grains", Astrophysical Journal, 217, 425 (1977)

[12] Wolf, S.,"Efficient Radiative Transfer in Dust Grain Mixtures", Astrophysical Journal, 582, 859 (2003).

[13] Chiavassa, A., Plez, B., Josselin, E., Freytag, B., "Radiative hydrodynamics simulations of red supergiant stars. I. interpretation of interferometric observations" Astronomy and Astrophysics, 506, 1351 (2009)

[14] Freytag, B. & Hofner, S., "Three-dimensional simulations of the atmosphere of an AGB star" Astronomy and Astrophysics, 483, 571 (2008).